PCCP

PAPER

View Article Online
View Journal

Cite this: DOI: 10.1039/c7cp03619a

A chemometric approach for determining the reaction quantum yields in consecutive photochemical processes†

Juan P. Marcolongo, Juan Schmidt, Natalia Levin and Leonardo D. Slep*

A chemometric procedure to deal with spectroscopically monitored processes involving photochemical steps is fully described. The methodology makes it possible to work with reactions that involve several components with unknown (and eventually overlapping) spectra and provides a tool for the simultaneous determination of both the quantum yields of the reaction and the spectra of all the species present in a multi-step photochemical process. As a benchmark, we apply these ideas to extract the quantum yields of photodetachment of coordinated ligands employing data recorded over the course of the decomposition of $[Ru(tpm)(bpy)(CH_3CN)]^{2+}$ and *cis*-$[Ru(bpy)_2(CH_3CN)_2]^{2+}$ under stationary photolysis conditions. The approach is fast and robust and it is easily implemented in scientific programming languages.

Received 29th May 2017,
Accepted 25th July 2017

DOI: 10.1039/c7cp03619a

rsc.li/pccp

Introduction

The determination of the quantum yield associated with photochemical processes has been of fundamental concern to the community since the discovery of the fact that excited states may have a different reactivity behavior than the same systems in their ground states.[1–4] This task can be straightforward when the incident radiation interacts with the reactant and not with the reaction's product, but may rapidly become complicated if other components in the reaction mixture (products, intermediates, or even spectator molecules) absorb light at the excitation wavelength. The so-called ''inner filter effect'', relevant not only in photochemistry but also in photophysics (and potentially in analytical chemistry), is something to be aware of in any quantitative photochemical determination. The brute force approach often employed in quantum yield determinations involves the elimination of any colored interference, something that can be achieved if the processes are studied at the low conversion limit. This strategy however may be impractical in many cases where the reactions are monitored spectrophotometrically. Sometime ago,[5] a quantitative procedure to account for the accumulation of a colored product over the course of a quantum yield (ϕ) determination experiment was proposed in the literature. The key to deal with the increasing fraction of light absorbed by the product is a clever use of eqn (1), where C_R stands for the concentration of the reactant, A_t and ε_R correspond to the absorbance of the solution and the extinction coefficient of the reactant at the excitation wavelength, respectively, and b is the pathlength. This equation can be rearranged to yield a linear expression that allows the evaluation of ϕ, as in eqn (2).

$$-\frac{dC_R}{dt} = \phi I_0\left(1 - 10^{-A_t}\right)\frac{\varepsilon_R b C_R}{A_t} \quad (1)$$

$$\ln\left(\frac{C_R}{C_R^0}\right) = -\phi I_0 \varepsilon_R b \int_{t_0}^{t_1}\left[\frac{\left(1 - 10^{-A_t}\right)}{A_t}\right]dt \quad (2)$$

The left-hand side of eqn (2), related to the fraction of remaining reactant at any point of the process, can be spectrophotometrically evaluated in a single wavelength determination by eqn (3), where the absorbances A_t, A_∞, and A_0 correspond to the wavelength at which the reaction is being monitored. The right-hand side of the expression requires numerical integration of the experimental data, and is therefore dependent on the time-step employed when recording the experiment.

$$\ln\left(\frac{C_R}{C_R^0}\right) = \ln\left(\frac{A_t - A_\infty}{A_0 - A_\infty}\right) \quad (3)$$

Since then, this method has become the standard to deal with this effect and essentially no further developments have been proposed. In our daily research investigations of coordination compounds[6–10] we faced many of its limitations: (i) the

Departamento de Química Inorgánica, Analítica y Química Física, Facultad de Ciencias Exactas y Naturales, and INQUIMAE, Universidad de Buenos Aires – CONICET, Pabellón 2, 3er piso, Ciudad Universitaria, C1428EHA Ciudad Autónoma de Buenos Aires, Argentina. E-mail: slep@qi.fcen.uba.ar

† Electronic supplementary information (ESI) available. See DOI: 10.1039/c7cp03619a

methodology has all the drawbacks associated with single wavelength quantifications; (ii) several interesting photoreactions proceed in a multistep fashion, so the time-dependent concentrations of all the components present in the solution require additional differential equations that do not allow a linearization of the *A vs. t* traces; (iii) the rate of the different photochemical processes in a multistep mechanism is determined by the fraction of light absorbed by the intermediates, apparently requiring *a priori* knowledge of their extinction coefficients; (iv) most transient colored intermediate species cannot be prepared in an independent procedure, therefore knowing their spectra might be an objective in itself; in clear collision with (iii).

As a matter of fact, (i) and (ii) apply not only to light-driven processes, but are actual complications experienced in many other determinations (*e.g.*, evaluation of equilibrium and kinetic constants, speciation of metal ions in solution, spectroelectrochemical characterization of redox active species, *etc.*). Chemometrics has provided a powerful approach to deal with these issues by using multiwavelength (and more generally multichannel) acquisition instruments, which allow the collection of an $N_M \times N_\lambda$ data matrix $\mathbf{A}_{exp}$ comprising N_M measurements at N_λ wavelengths (channels). In the analysis of all such experiments, the primary goal is the decomposition of the original matrix $\mathbf{A}_{exp}$ into two smaller matrices: containing the $N_M \times N_S$ concentration profiles **C** matrix (N_S = number of evolving species) and the $N_S \times N_\lambda$ array of individual spectra **E** as in eqn (4), where the pathlength b = 1.00 cm has been dropped (see Table S1 (ESI†) for a complete list of symbols employed in this manuscript):

$$\mathbf{A}_{exp} = \mathbf{C} \times \mathbf{E} \quad (4)$$

The decomposition relies on two strong requirements: (a) linear response of the measuring equipment to the individual concentrations (validity of Beer's law) and (b) a proper description of the concentration profiles by means of a chemical model where equilibrium or kinetic constants, redox potentials, *etc.* can be treated as the fitting parameters of the model. In particular, the second condition restrains the set of possible **C** and **E** that satisfy eqn (4), which otherwise would be of infinite dimension.[11–16] The methodology has been largely and successfully employed in the last 30 years in many experimental situations, but to our knowledge there are no implementations dealing with some of the limitations (particularly (iii) and (iv)) described above. We report herein the fundamentals of a method that we have developed with potential application in many situations in the field.

Materials and experimental procedures

Materials and reagents

The reagents employed in the synthetic procedures were purchased from Sigma-Aldrich, and were used without further purification. All the organic solvents employed in the synthetic procedures or physical determinations were dried and freshly distilled before use following standard procedures. A vacuum line and Schlenk glassware (or alternatively a glovebox) were employed when the manipulation required exclusion of air. $[Ru(tpm)(bpy)(CH_3CN)](PF_6)_2$ (tpm = tris(1-pyrazolyl)methane, bpy = 2,2′-bipyridine), *cis*-$[Ru(bpy)_2(CH_3CN)_2](PF_6)_2$, and $K_3[Fe(C_2O_4)_3]$ were prepared and characterized as in (or introducing slight modifications of) the reported literature procedures.[17–19]

Physical determinations. Microanalytical data for C, H, and N were obtained with a Carlo Erba EA 1108 analyzer. UV-vis spectra were recorded with either an HP8453 or an HP8452A diode array spectrophotometer. The IR spectral measurements (KBr pellets) were carried out using a Nicolet iS10. The ^{1}H and ^{13}C NMR spectra were measured with a 500 MHz Bruker AM 500 spectrometer. The photochemical experiments were performed with 2.6 mL of solutions contained in a 1.00 cm pathlength fluorescence cuvette employing a 450 nm Light Emitting Diode (LED). The intensity of the 450 nm LED (2.70×10^{-6} einstein s^{-1} dm^{-3}) was determined by reference to a 365 nm LED source employing a FieldMaster–Coherent power meter with a LM-2UV photodiode as a light sensor. The 365 nm LED was calibrated by actinometry employing a standard solution of $K_3[Fe(C_2O_4)_3]$ by means of an already-described procedure,[20] yielding an intensity of 1.59×10^{-6} einstein s^{-1} dm^{-3}. The spectral evolution was monitored spectrophotometrically along the course of the reaction in a 90° configuration.

Fundamentals of the procedure applied to photochemical processes

Photochemical reactions differ from purely thermal processes in the fact that their rates depend on the fraction of light absorbed by the different reactants. The concentration profile for a thermal process can be usually modeled by a set of differential equations built upon an explicit inclusion of an adequate number of parameters (from now on "the chemical model"). For a reaction mixture of N_S species that require K parameters to build the chemical model, the concentration profiles c_i can be described by

$$c_i(\xi) = f(\xi, \{p_1, p_2, \ldots, p_K\}) \quad (5)$$

where ξ stands for time, pH, redox potential, or other relevant variables, depending on the system of interest. In a photochemical reaction model the set of extinction coefficients $\{\varepsilon_1 \ldots \varepsilon_{N_S}\}$ is also required to evaluate the fraction of light absorbed by the reactant species

$$c_i(\xi) = f(\xi, \{p_1, p_2, \ldots, p_K\}, \{\varepsilon_1 \ldots \varepsilon_{N_S}\}) \quad (6)$$

Independently of the thermal or photochemical nature of the process, we describe here strategies to recover the set of parameters that provide the best fit of the proposed chemical model to the actual experimental data contained in matrix **A**. Different situations arise, depending on the available information.

Case I *the spectra of all the species in the reacting system are known*

If the spectra of all the components can be obtained independently and arranged in a $N_S \times N_\lambda$ matrix $\mathbf{E}_{exp}$, the problem is solved in a straightforward manner. Several approaches have

been described in the literature[11–16] requiring, in the general case, an iterative procedure. Different approximations differ in the method chosen to evaluate the goodness of fit.

First alternative:

Step 1: the "experimental" concentration profiles can be computed by least squares[21–23] as in eqn (7), provided that the rows of $\mathbf{E}_{exp}$ are linearly independent:

$$\mathbf{C}_{exp} = \mathbf{A}_{exp} \times \mathbf{E}_{exp}^{t} \times \left(\mathbf{E}_{exp} \times \mathbf{E}_{exp}^{t}\right)^{-1} \quad (7)$$

Step 2: a set of parameters $\{p_1 \ldots p_K\}$ is chosen as an initial guess for the fitting procedure.

Step 3: the concentration profiles predicted by this set of parameters are computed as in eqn (5) or (6) depending on the nature of the process. These profiles can be arranged in an array $\mathbf{C}$ whose dimensions are $N_M \times N_S$ (one column per species, one line for each value of ξ).

Step 4: $\mathbf{C}_{exp}$ and $\mathbf{C}$ are compared to evaluate the deviation between the predicted and the experimental concentration profiles (eqn (8)).

$$\Omega_C = \left[\sum_{i,j}\left(\left(\mathbf{C} - \mathbf{C}_{exp}\right)_{ij}\right)^2\right]^{\frac{1}{2}} \quad (8)$$

Depending on the value of Ω_C, a new set of parameters has to be chosen and all the steps between 2 and 4 have to be repeated until the deviation between $\mathbf{C}$ and $\mathbf{C}_{exp}$ reaches a minimum. This procedure allows the best set of fitting parameters $\{p_1 \ldots p_K\}$ to be obtained.

Second alternative:

Step 1: a set of parameters $\{p_1 \ldots p_K\}^{\circ}$ is chosen as an initial guess for the fitting procedure.

Step 2: the concentration profiles predicted by this set of parameters are computed as in eqn (5) or (6) depending on the nature of the process. These profiles can be arranged in an array $\mathbf{C}$ whose dimensions are $N_M \times N_S$.

Step 3: the predicted spectral evolution array for the computed concentration profiles can be evaluated by

$$\mathbf{A} = \mathbf{C} \times \mathbf{E}_{exp} \quad (9)$$

Step 4: $\mathbf{A}$ and $\mathbf{A}_{exp}$ are compared in order to evaluate the deviation between the experimental and predicted values:

$$\Omega_A = \left[\sum_{i,j}\left(\left(\mathbf{A}_{exp} - \mathbf{A}\right)_{ij}\right)^2\right]^{\frac{1}{2}} \quad (10)$$

Depending on the value of Ω_A, a new set of parameters has to be chosen and all the steps between 2 and 4 have to be repeated until the deviation between $\mathbf{A}_{exp}$ and $\mathbf{A}$ reaches a minimum.

In the ideal situation where experimental noise is absent, both the alternatives based on the minimization of Ω_C and Ω_A yield virtually the same optimized $\{p_1 \ldots p_K\}$ set. However, in real situations, the results might be noncoincident. In many early implementations of chemometric tools,[12–16] the strategy essentially based on the minimization of Ω_C was preferred, due to the smaller size of the arrays describing the concentration profiles, a constraint introduced by the computational resources available. Nowadays this is no longer a limitation, and the second alternative is perfectly achievable in any personal computer. Actually, its implementation (particularly reactions comprising photochemical steps in which the spectra of the colored species are not known) is rather straightforward. In the rest of the manuscript, and also in Fig. 1, which resumes the different situations and algorithms described in the manuscript, we will refer only to this possibility, though the traditional alternative of optimizing Ω_C can also be implemented.

Case II: *purely thermal process with unknown spectral characteristics of the species in the reacting system*

The lack of knowledge of the spectra precludes the direct computation of $\mathbf{A}$ based on the concentration profiles derived from the chemical model. However, there is still a general procedure to deal with this situation that will provide not only the set of parameters that provide the best fit to the proposed chemical model to the actual experimental data contained in matrix $\mathbf{A}$, but also the deconvoluted individual spectra of the colored species. The iterative procedure, also resumed in Fig. 1, requires the following steps:

Step 1: a set of parameters $\{p_1 \ldots p_K\}^{\circ}$ is chosen as an initial guess for the fitting procedure.

Step 2: the concentration profiles are computed as in eqn (5). These profiles can be arranged in an array $\mathbf{C}$ whose dimensions are $N_M \times N_S$ (one column per species, one line for each value of ξ).

Step 3: if the concentration profiles are linearly independent, the spectra of the N_S components of the mixture that best describe (in the least squares sense)[21–23] the spectral evolution along the experiment for this particular set $\{p_1 \ldots p_K\}$ can be computed as:

$$\mathbf{E} = \left(\mathbf{C}^{t} \times \mathbf{C}\right)^{-1} \times \mathbf{C}^{t} \times \mathbf{A}_{exp} \quad (11)$$

Step 4: $\mathbf{C}$ and $\mathbf{E}$ are employed to compute the predicted spectral evolution and compare it with the experimental one.

$$\mathbf{A} = \mathbf{C} \times \mathbf{E} \quad (12)$$

Depending on the value of Ω_A (computed here as in eqn (10)), a new set of parameters has to be chosen and all the steps between 2 and 4 have to be repeated iteratively until the deviation between $\mathbf{A}$ and $\mathbf{A}_{exp}$ reaches a minimum. This procedure allows the best set of fitting parameters $\{p_1 \ldots p_K\}$ and the spectra of the colored species to be obtained, which are not required for the analysis.

Case III: *mixed thermal and photochemical processes with unknown spectral characteristics of the species in the reacting system*

Any attempt to employ the above strategy to processes involving photochemical steps would fail because, as mentioned before, in a photochemical reaction model the set of extinction coefficients $\{\varepsilon_1 \ldots \varepsilon_{N_S}\}$ is required to evaluate the fraction of light absorbed by the reactant species at the irradiation wavelength. This complication can be circumvented in a double loop iteration procedure depicted in Fig. 1, and described in the following, that provides both $\{p_1 \ldots p_K\}$ and the spectra of the different colored species $\{\varepsilon_1 \ldots \varepsilon_{N_S}\}$ as an outcome.

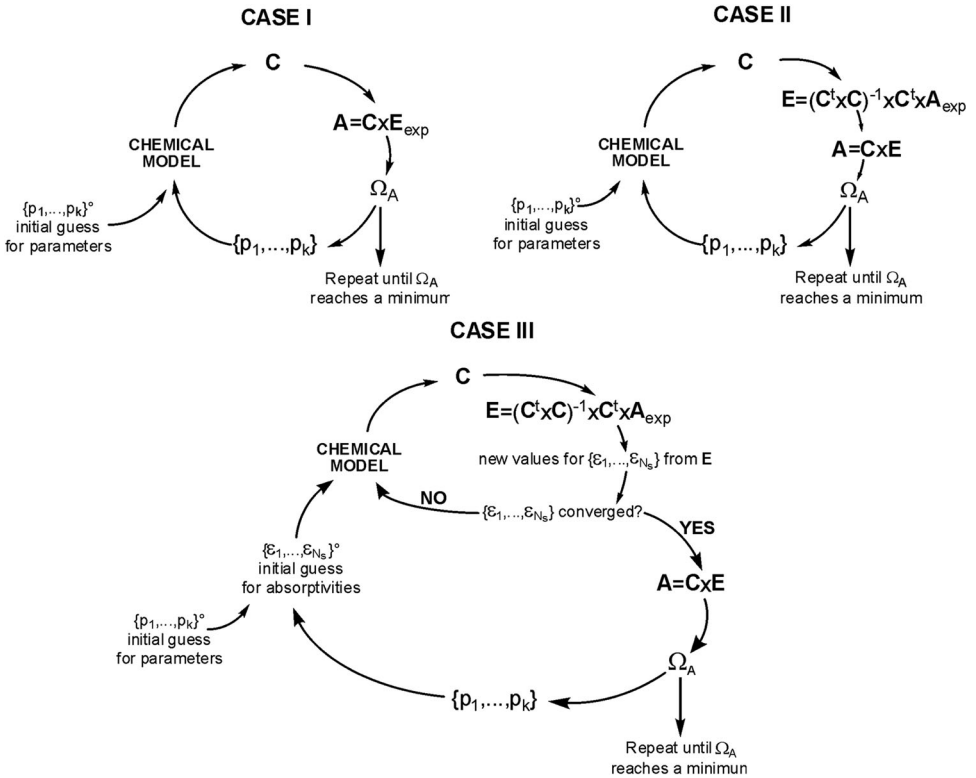

Fig. 1 Schematic representation of the iterative procedures performed in the different cases described along the manuscript.

Step 1: a set of parameters $\{p_1 \ldots p_K\}^\circ$ has to be chosen as an initial guess for the fitting procedure.

Step 2: an initial estimation of $\{\varepsilon_1 \ldots \varepsilon_{N_S}\}$ has to be provided in order to compute the evolution of the species over the course of the irradiation time. This is normally not difficult for ε_1, which corresponds to the reactant. For the remaining species the values for the first iteration step can be established in many ways, sometimes from the inspection of the experimental absorption profiles, and better estimations will progressively result along the computations.

Step 3: the concentration profiles associated with this particular set of parameters $\{p_1 \ldots p_K\}$ and $\{\varepsilon_1 \ldots \varepsilon_{N_S}\}$ are computed as in eqn (6). These profiles can be arranged in an $N_M \times N_S$ matrix **C**.

Step 4: the spectra of the N_S components of the mixture that best describe (in the least squares sense) the spectral evolution along the experiment for this particular set $\{p_1 \ldots p_K\}$ can be computed with eqn (11).

This new matrix **E** contains a new set of absorptivities $\{\varepsilon_1 \ldots \varepsilon_{N_S}\}$ that becomes the new input for the concentration profile computation, still keeping the same values for the fitting parameters of the chemical model $\{p_1 \ldots p_K\}$. Steps 3 and 4 have to be repeated until invariance of the spectra described by eqn (11). This condition is fulfilled when the quadratic norm of the difference between the computed spectra obtained in the two consecutive iteration processes results in less than an arbitrary value, for instance the one arising solely from the uncertainty of the instrument. Only when the termination condition for this inner loop is achieved (see Fig. 1) is it possible to proceed to the following step.

Step 5: the **C** and **E** arrays are employed to compute the predicted spectral evolution and compare it with the experimental one using eqn (12) and (10).

Depending on Ω_A, a new set of parameters $\{p_1 \ldots p_K\}$ has to be chosen and all the steps between 3 and 5 have to be repeated. Note that at this point, the $\{\varepsilon_1 \ldots \varepsilon_{N_S}\}$ is no longer the one proposed in step 2, but actually a refined set resulting from the inner loop iteration. The outer loop computation has to be repeated until the deviation between **A** and $\mathbf{A}_{exp}$ reaches a minimum. This procedure allows the best set of fitting parameters $\{p_1 \ldots p_K\}$ and $\{\varepsilon_1 \ldots \varepsilon_{N_S}\}$ (the spectra of the colored species) to be obtained, which are not required to be known at the beginning of the analysis.

Examples of application

In the following examples, we will explore the application of these ideas to two well-defined photochemical processes. On one hand, we will study the substitution of an acetonitrile molecule (CH_3CN) by H_2O, following the irradiation of $[Ru(tpm)(bpy)(CH_3CN)]^{2+}$ in aqueous solution. This species has been reported by Katz and coworkers[18] and has been chosen because of its ease of preparation and characterization and its thermal inertness towards ligand substitution and other processes in neutral aqueous solutions. The second application involves the photosubstitution of CH_3CN by H_2O in *cis*-$[Ru(bpy)_2(CH_3CN)_2]^{2+}$, one of the examples included in the keystone report by Pinnick and Durham,[24] and more recently employed in the context of an ultrafast spectroscopy exploration of the system.[25]

(a) Photosubstitution in $[Ru(tpm)(bpy)(CH_3CN)]^{2+}$: an A → B process

Solutions of $[Ru(tpm)(bpy)(CH_3CN)]^{2+}$ in water remain unchanged for prolonged periods.[18] In contrast, rapid spectral changes are detected once the solutions are irradiated with a 450 nm LED and eventually lead to full conversion. Fig. 2 displays the spectral evolution along the irradiation time, with well-defined isosbestic points over the course of the reaction, which can be described as

$$[Ru(tpm)(bpy)(CH_3CN)]^{2+} + H_2O \xrightarrow[\phi]{h\nu} [Ru(tpm)(bpy)(H_2O)]^{2+} + CH_3CN \quad (13)$$

The identity of the aquo-product can unambiguously be determined by a comparison of its spectral characteristics with those reported for $[Ru(tpm)(bpy)(H_2O)]^{2+}$,[26] (*cf.* Fig. 3). The absence of side reactions or any other species that might interfere in the absorption of light allows the observed changes to be described by means of the following equations (the "chemical model"):

$$C_R + C_P = C_0 \quad (14)$$

$$-\frac{dC_R}{dt} = \frac{dC_P}{dt} = \phi I_0 (1 - 10^{-A_t}) \frac{\varepsilon_R C_R}{\varepsilon_R C_R + \varepsilon_P C_P} \quad (15)$$

C_0 stands for the analytical concentration of $[Ru(tpm)(bpy)(CH_3CN)]^{2+}$ at the beginning of the experiment, while C_R, ε_R and C_P, ε_P represent the concentrations and extinction coefficients of $[Ru(tpm)(bpy)(CH_3CN)]^{2+}$ and $[Ru(tpm)(bpy)(H_2O)]^{2+}$, respectively. In this particular example, and recalling the symbols employed in eqn (6), $\xi = t$, while there is only a single parameter $p_1 = \phi$. Note that eqn (15) (which can be easily derived from eqn (1)) requires not only the evaluation of A_t, ε_R and ε_P at the excitation wavelength but also a strictly monochromatic excitation source. Under our experimental conditions the irradiation has been performed with a *ca.* 20 nm FWHM LED (see Fig. 2) so that eqn (15) needs to be replaced by the following expression,

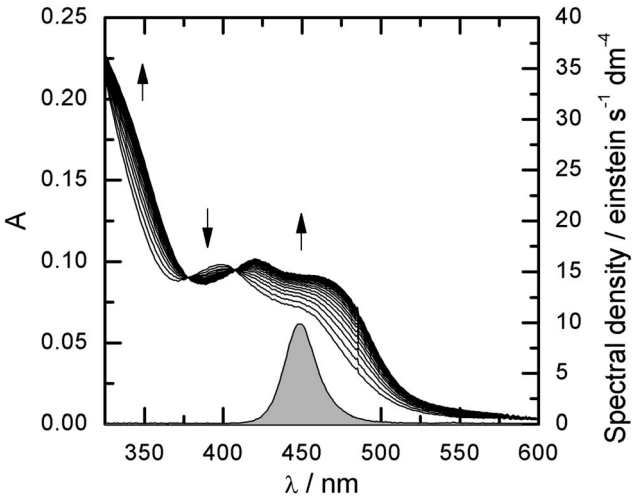

Fig. 2 Spectral evolution over the course of the irradiation of $[Ru(tpm)(bpy)(CH_3CN)]^{2+}$ in water. Δt = 30 s. The spectrum shaded in gray corresponds to the spectral density of the irradiation source.

where the polychromatic nature of the irradiation source is explicitly taken into account:

$$-\frac{dC_R}{dt} = \frac{dC_P}{dt} = \phi \int I_0(\lambda) \left(1 - 10^{-A_t(\lambda)}\right) \frac{\varepsilon_R(\lambda) C_R}{\varepsilon_R(\lambda) C_R + \varepsilon_P(\lambda) C_P} d\lambda \quad (16)$$

The quantum yield of the process (ϕ) is the only fitting parameter of the chemical model and has been assumed to be independent of the wavelength throughout the bandwidth of the LED. This assumption is reasonable provided that only one absorption band is observable in the range covered by the photolysis source. The resulting differential equation cannot be solved algebraically, but there are efficient algorithms that provide discrete values for the concentrations at intervals determined by the experimental conditions. In our implementation (*cf.* the ESI† Section for details) we preferred the fourth-order Runge–Kutta method.[27] The nature of the system (full *a priori* knowledge of the absorption profiles for both the colored species) allows for the optimization of ϕ as described above in Case I. Fig. 3 depicts the quadratic residual between the predicted and experimental absorption profiles (see eqn (10)) showing a single minimum, which corresponds to ϕ = 0.32 mol einstein^{-1}. The iterative exploration can be initiated from different values of ϕ, and only a few steps of a Levenberg–Marquardt nonlinear iterative fitting procedure[28] are required to reach the minimum, as demonstrated in Fig. 3.

The same set of experimental data can be treated with the methodology developed by us for reactions in which the spectra of the components are unknown (Case III situation). The fact that the actual spectra are known turns this system into a well-suited benchmark to validate the methodology. Fig. 4 and Fig. S1, S2 (ESI†) display the quadratic error response, together with the paths followed along the minimization procedure for different initial conditions: different initial ϕ-values and/or different estimations of the individual spectra are required as initial guesses to start the optimization procedure. Note that the initial choice of ϕ (smaller or larger than the optimum one) or the spectra (a clever one as, for instance, the initial and final spectra of the experiment that is essentially a complete one-step reaction, or a poorer one like assuming that the products are completely uncolored) has a very small influence on the number of iterations required to reach the optimized values and renders exactly the same final estimation of the spectra and ϕ = 0.32 mol einstein^{-1}. Both are in excellent agreement with those computed employing the spectra of the pure species.

(b) Photosubstitution in *cis*-$[Ru(bpy)_2(CH_3CN)_2]^{2+}$: a two-step A → B → C process

The coordination compounds containing the $\{Ru(bpy)_2\}^{2+}$ fragment have been known to undergo photoinduced ligand exchange since the early work by Pinnick and Durham.[24] These species have been employed in fundamental research and as potential cage compounds[29–32] for the delivery of small molecules and for assessing the effect these molecules might trigger on living tissues, studies that could eventually lead to applications in photodynamic therapy (PDT). *cis*-$[Ru(bpy)_2(CH_3CN)_2]^{2+}$ itself

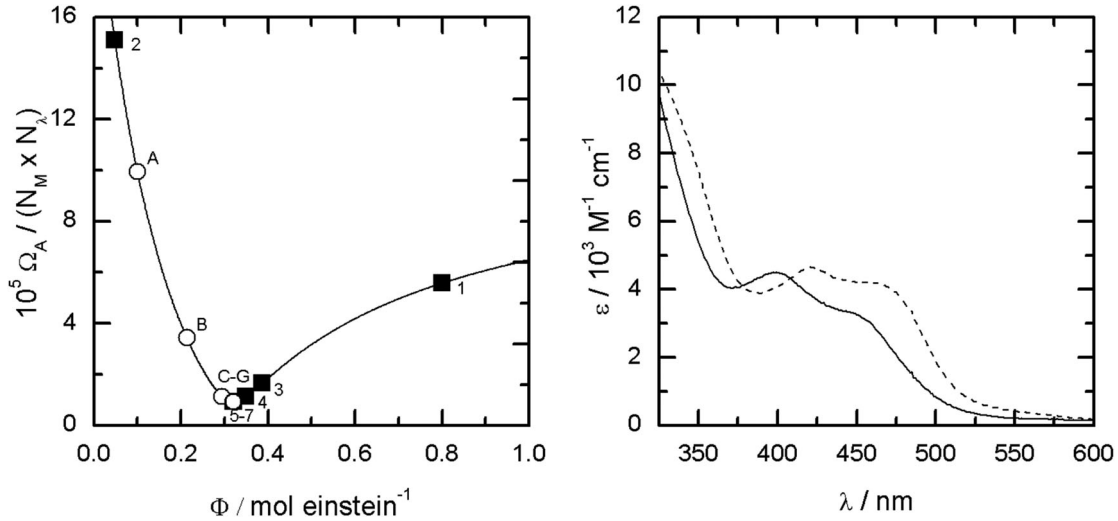

Fig. 3 Evolution of Ω_A during the iterative minimization procedure for two different initial values of the fitting parameter ϕ = 0.8 mol einstein^{-1} (squares) and 0.1 mol einstein^{-1} (circles) in an A → B process (left). Spectra of the reactant (solid line) and product (dashed line) obtained from pure samples (right). λ_{irr} = 450 nm, see Fig. 2 for the spectral density of the irradiation source.

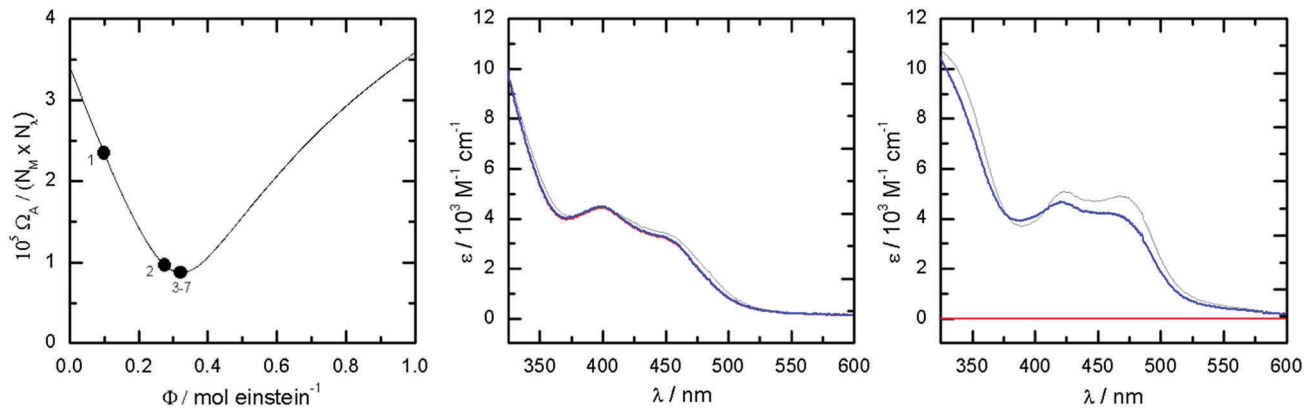

Fig. 4 Evolution of Ω_A during the iterative minimization procedure with unknown spectra for the colored species in an A → B process using $\phi_{initial}$ = 0.1 mol einstein^{-1} (left). Spectral changes along the iteration steps for the reactant (middle) and product (right). Initial guess colored in red, spectrum after the last iteration in blue. λ_{irr} = 450 nm, see Fig. 2 for the spectral density of the irradiation source.

has been employed in conjunction with other *cis*-$[Ru(bpy)_2X_2]^{n+}$ species to disclose the mechanism involved in the photorelease of one ligand of the coordination sphere from the lowest energy ^{3}d–d state, which is usually thermally populated from the lower lying ^{3}MLCT after direct irradiation of an MLCT absorption band in the visible region of the spectrum.[24]

Solutions of *cis*-$[Ru(bpy)_2(CH_3CN)_2]^{2+}$ in water remain unchanged for prolonged periods, showing that the species is inert towards ligand substitution. Steady-state irradiation of *cis*-$[Ru(bpy)_2(CH_3CN)_2]^{2+}$ in water results in the stepwise replacement of both the CH_3CN ligands with H_2O.[25] The formation of the mono-aqua intermediate, *cis*-$[Ru(bpy)_2(CH_3CN)(H_2O)]^{2+}$ (eqn (17)) with ϕ_1 = 0.31 mol einstein^{-1}, has been assigned to the changes observed at early times of photolysis with λ_{irr} = 436 nm.[24] This interpretation was subsequently supported[25] in an experiment that showed the transient appearance of a maximum at ~458 nm. The formation of the bis-aqua product, *cis*-$[Ru(bpy)_2(H_2O)_2]^{2+}$ from the intermediate species (eqn (18)) requires longer irradiation times, and to our knowledge its quantum yield has never been reported.

$$cis\text{-}\left[Ru(bpy)_2(CH_3CN)_2\right]^{2+} + H_2O \xrightarrow[\phi_1]{h\nu} cis\text{-}\left[Ru(bpy)_2(CH_3CN)(H_2O)\right]^{2+} + CH_3CN \quad (17)$$

$$cis\text{-}\left[Ru(bpy)_2(CH_3CN)(H_2O)\right]^{2+} + H_2O \xrightarrow[\phi_2]{h\nu} cis\text{-}\left[Ru(bpy)_2(H_2O)_2\right]^{2+} + CH_3CN \quad (18)$$

Fig. 5 displays the spectral changes recorded in the stationary photolysis of *cis*-$[Ru(bpy)_2(CH_3CN)_2]^{2+}$ at 450 nm. Singular value decomposition[33] of the experimental **A** matrix suggests that it should be possible to model the spectral evolution with only three colored species,[34–36] in agreement with the previous

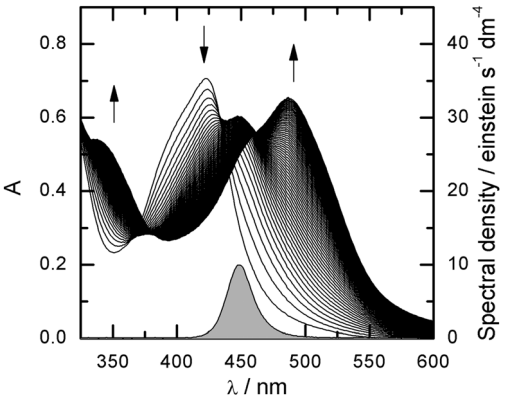

Fig. 5 Spectral profile evolution upon irradiation of *cis*-$[Ru(bpy)_2(CH_3CN)_2]^{2+}$ in water. Δt = 30 s. The spectrum shaded in gray corresponds to the spectral density of the irradiation source.

reports described above. The spectral evolution strongly resembles that reported in the literature,[25] and the spectrum of a solution irradiated until no further spectral changes were observed became identical to that reported for the bis-aqua complex *cis*-$[Ru(bpy)_2(H_2O)_2]^{2+}$,[37] establishing the identity of the final product without any possible ambiguities. The chemical model employed in this case to compute the temporal evolution involves the following set of differential equations, which are the natural extension of eqn (14)–(16) to a two-step reaction mechanism:

$$C_R + C_I + C_P = C_0 \quad (19)$$

$$-\frac{dC_R}{dt} = \phi_1 \int I_0(\lambda)\left(1 - 10^{-A_t(\lambda)}\right)\frac{\varepsilon_R(\lambda)C_R}{\varepsilon_R(\lambda)C_R + \varepsilon_I(\lambda)C_I + \varepsilon_P(\lambda)C_P}d\lambda \quad (20)$$

$$\frac{dC_I}{dt} = \int I_0(\lambda)\left(1 - 10^{-A_t(\lambda)}\right)\frac{\phi_1\varepsilon_R(\lambda)C_R - \phi_2\varepsilon_I(\lambda)C_I}{\varepsilon_R(\lambda)C_R + \varepsilon_I(\lambda)C_I + \varepsilon_P(\lambda)C_P}d\lambda \quad (21)$$

Here, the subindexes R, I, and P stand for *cis*-$[Ru(bpy)_2(CH_3CN)_2]^{2+}$, *cis*-$[Ru(bpy)_2(CH_3CN)(H_2O)]^{2+}$, and *cis*-$[Ru(bpy)_2(H_2O)_2]^{2+}$, respectively, whereas all the other symbols have the same meaning as in eqn (16). This set of equations can be solved numerically for any values of $\{p_1, p_2\} = \{\phi_1, \phi_2\}$ and the extinction coefficients, making this system suitable to be analyzed as a Case III situation. Fig. 6 and Fig. S3, S4 (ESI†) show the contour plots of $\Omega_A(\phi_1, \phi_2)$ in the vicinities of its minimum value and several trajectories that reveal that independently of the initial ϕ_1 and ϕ_2 values and the absorption spectra for the three colored species proposed as an initial guess for the iterative procedure, the minimum is reached in only a few iterations that consistently provide the same quantum

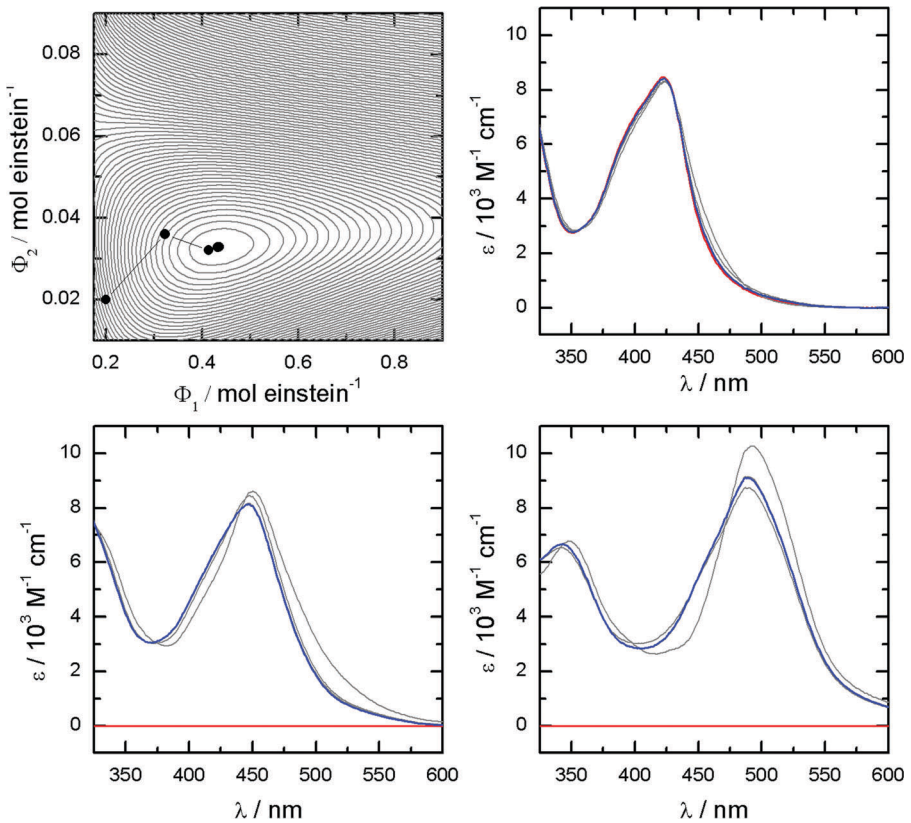

Fig. 6 Evolution of Ω_A during the iterative minimization procedure with unknown spectra for the colored species in an A → B → C process. Initial values for ϕ_1 = 0.2 mol einstein^{-1} and ϕ_2 = 0.02 mol einstein^{-1} (upper left). The contour plot corresponds to $\Delta\Omega_A/(N_M \times N_\lambda) = 1 \times 10^{-5}$. Spectral changes along the iteration steps for the reactant (upper right), intermediate (lower left), and product species (lower right). Initial guess colored in red, spectrum after the last iteration in blue. λ_{irr} = 450 nm, see Fig. 5 for the spectral density of the irradiation source.

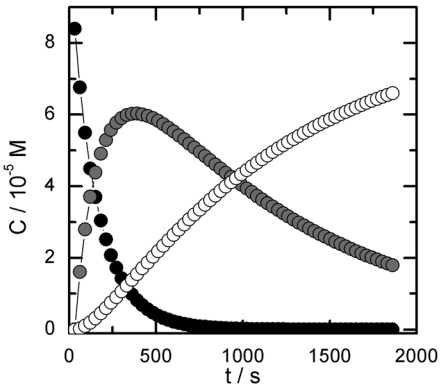

Fig. 7 Calculated concentration profiles of reactant, intermediate, and product species over the course of the photodecomposition of *cis*-$[Ru(bpy)_2(CH_3CN)_2]^{2+}$ in water. Δt = 30 s. λ_{irr} = 450 nm, see Fig. 2 for the spectral density of the irradiation source.

yields (ϕ_1 = 0.44 mol einstein^{-1}, ϕ_2 = 0.033 mol einstein^{-1}) and deconvoluted spectra (Fig. 6). The concentration profile associated with these values (Fig. 7) reveals that even shortly after starting the photolysis there are measurable amounts of the three species in the solution, a possible explanation for the discrepancy between our value for ϕ_1 and the one from ref. 24 obtained under the assumption of a single isolated photoreaction involving only two colored species.

Conclusions

We propose an approach to deal with processes that involve photochemical steps. We have provided background and details to recover quantum yield values from stationary photolysis experiments, even when the absorption spectra of the components are *a priori* not known. The example chosen for a simple A → B process reveals that this methodology yields quantitative results that are as reliable as those obtained by using the actual absorption profiles of the species. In a more complex A → B → C reaction (and eventually in any kind of process that requires photochemical steps to describe a chemical model that might also involve thermally driven steps), the method proves valuable to reveal the spectral characteristics of the intermediates. As with any iterative optimization procedure, the choice of the initial conditions for the iteration may be crucial to guarantee its success. Nevertheless, we have shown that, to some extent, the method is not particularly sensitive to the initial estimation of the extinction coefficients of the different colored species. In our experience, the computational cost is minimal with typical fitting times in the range of tenths of seconds. Summing up, we feel that this is an attractive tool that should be easily implemented by anyone familiar with scientific programming languages in any modern personal computer.

Acknowledgements

This work has been supported by grants from CONICET, ANPCyT, and the University of Buenos Aires (UBA). LDS is a member of the scientific staff of CONICET. JPM and NL are postdoctoral and doctoral fellows, respectively, of the same Institution while JS hold an undergraduate research scholarship from UBA. The authors wish to thank Dr E. Morzán and Dr José Hodak for fruitful discussions and careful reading of the manuscript.

References

1 R. P. Wayne, *Principles and Applications of Photochemistry*, Oxford University Press, Oxford, 1988.
2 B. Wardle, *Principles and Applications of Photochemistry*, John Wiley & Sons, Ltd, Great Britain, 1st edn, 2009.
3 J. R. Lakowicz, *Principles of Fluorescence Spectroscopy*, Springer Science + Business Media, LLC, Singapore, 3rd edn, 2006.
4 G. Stochel, M. Brindell, W. Macyk, Z. Stasicka and K. Szacilowski, *Bioinorganic Photochemistry*, John Wiley & Sons Ltd, Singapore, 2009.
5 A. J. Lees, *Anal. Chem.*, 1996, **68**, 226–229.
6 A. Petroni, L. D. Slep and R. Etchenique, *Inorg. Chem.*, 2008, **47**, 951–956.
7 A. G. De Candia, J. P. Marcolongo, R. Etchenique and L. D. Slep, *Inorg. Chem.*, 2010, **49**, 6925–6930.
8 J. P. Marcolongo, T. Weyhermuller and L. D. Slep, *Inorg. Chim. Acta*, 2015, **429**, 174–182.
9 N. Levin, N. O. Codesido, E. Bill, T. Weyhermueller, A. P. S. Gaspari, R. S. da Silva, J. A. Olabe and L. D. Slep, *Inorg. Chem.*, 2016, **55**, 7808–7810.
10 L. C. B. Ramos, M. S. P. Marchesi, D. Callejon, M. D. Baruffi, C. N. Lunardi, L. D. Slep, L. M. Bendhack and R. S. da Silva, *Eur. J. Inorg. Chem.*, 2016, 3592–3597.
11 H. Gampp, M. Maeder, C. J. Meyer and A. D. Zuberbühler, *Anal. Chim. Acta*, 1987, **193**, 287–293.
12 H. Gampp, M. Maeder, C. J. Meyer and A. D. Zuberbühler, *Talanta*, 1985, **32**, 95–101.
13 H. Gampp, M. Maeder, C. J. Meyer and A. D. Zuberbühler, *Talanta*, 1985, **32**, 257–264.
14 H. Gampp, M. Maeder, C. J. Meyer and A. D. Zuberbühler, *Talanta*, 1985, **32**, 1133–1139.
15 M. Kubista, R. Sjoeback and B. Albinsson, *Anal. Chem.*, 1993, **65**, 994–998.
16 J. Nygren, J. M. Andrade and M. Kubista, *Anal. Chem.*, 1996, **68**, 1706–1710.
17 C. G. Hatchard and C. A. Parker, *Proc. R. Soc. London, Ser. A*, 1956, **235**, 518–536.
18 N. E. Katz, F. Fagalde, N. D. Lis De Katz, M. G. Mellace, I. Romero, A. Llobet and J. Benet-Buchholz, *Eur. J. Inorg. Chem.*, 2005, 3019–3023.
19 G. M. Brown, R. W. Callahan and T. J. Meyer, *Inorg. Chem.*, 1975, **14**, 1915–1921.
20 T. Lehóczki, É. Jôzsa and K. Ösz, *J. Photochem. Photobiol., A*, 2013, **251**, 63–68.
21 R. Penrose, *Math. Proc. Cambridge Philos. Soc.*, 1956, **52**, 17–19.

22 W. Edwards Deming, *Statistical Adjustment of Data*, John Wiley & Sons, Inc., New York, 4th edn, 1948.
23 D. L. Massart, B. G. M. Vandeginste, S. N. Deming, Y. Michotte and L. Kaufman, *Chemometrics: a Textbook*, Elsevier, Amsterdam, 5th edn, 2003.
24 D. V. Pinnick and B. Durham, *Inorg. Chem.*, 1984, **23**, 1440–1445.
25 Y. Liu, D. B. Turner, T. N. Singh, A. M. Angeles-Boza, A. Chouai, K. R. Dunbar and C. Turro, *J. Am. Chem. Soc.*, 2009, **131**, 26–27.
26 A. Llobet, *Inorg. Chim. Acta*, 1994, **221**, 125–131.
27 W. H. Press, B. P. Flannery, S. A. Teukolsky and W. T. Vetterling, in *Numerical Recipes in FORTRAN: The Art of Scientific Computing*, Cambridge University Press, Cambridge, England, 1992, ch. 16, pp. 704–716.
28 G. A. F. Seber and C. J. Wild, *Nonlinear Regression*, Wiley-Interscience, Hoboken (NJ), USA, 2003.
29 L. Zayat, C. I. Calero, P. Albores, L. M. Baraldo and R. Etchenique, *J. Am. Chem. Soc.*, 2003, **125**, 882–883.
30 L. Zayat, M. Salierno and R. Etchenique, *Inorg. Chem.*, 2006, **45**, 1728–1731.
31 L. Zayat, M. G. Noval, J. Campi, C. I. Calero, D. J. Calvo and R. Etchenique, *ChemBioChem*, 2007, **8**, 2035–2038.
32 E. M. Rial Verde, L. Zayat, R. Etchenique and R. Yuste, *Front. Neural Circuits*, 2008, **2**, 2.
33 E. R. Malinowski and D. G. Howery, *Factor Analysis in Chemistry*, Wiley-Interscience, New York, 1980.
34 E. R. Malinowski, *Anal. Chem.*, 1977, **49**, 606–612.
35 E. R. Malinowski, *Anal. Chem.*, 1977, **49**, 612–617.
36 E. R. Malinowski, *J. Chemom.*, 1988, **3**, 49–60.
37 B. Durham, S. R. Wilson, D. J. Hodgson and T. J. Meyer, *J. Am. Chem. Soc.*, 1980, **102**, 600–607.